

# *Contrasting fast precipitation responses to tropospheric and stratospheric ozone forcing*

Article

Published Version

Creative Commons: Attribution 4.0 (CC-BY)

Open access

MacIntosh, C. R., Allan, R. P., Baker, L. H., Bellouin, N., Collins, W., Mousavi, Z. and Shine, K. P. (2016) Contrasting fast precipitation responses to tropospheric and stratospheric ozone forcing. *Geophysical Research Letters*, 43 (3). pp. 1263-1271. ISSN 0094-8276 doi:  
<https://doi.org/10.1002/2015GL067231> Available at  
<https://centaur.reading.ac.uk/51463/>

It is advisable to refer to the publisher's version if you intend to cite from the work. See [Guidance on citing](#).

Published version at: <http://onlinelibrary.wiley.com/doi/10.1002/2015GL067231/abstract>

To link to this article DOI: <http://dx.doi.org/10.1002/2015GL067231>

Publisher: American Geophysical Union

All outputs in CentAUR are protected by Intellectual Property Rights law, including copyright law. Copyright and IPR is retained by the creators or other copyright holders. Terms and conditions for use of this material are defined in the [End User Agreement](#).

[www.reading.ac.uk/centaur](http://www.reading.ac.uk/centaur)

**CentAUR**

Central Archive at the University of Reading

Reading's research outputs online

## RESEARCH LETTER

10.1002/2015GL067231

## Key Points:

- Fast precipitation response to ozone change simulated in a global climate model
- Fast precipitation responses to tropospheric and stratospheric O<sub>3</sub> change oppose each other
- Simple model indicating present-day precipitation change due to O<sub>3</sub> could exceed 50% of that from CO<sub>2</sub>

## Supporting Information:

- Supporting Information S1

## Correspondence to:

K. P. Shine,  
k.p.shine@reading.ac.uk

## Citation:

MacIntosh, C. R., R. P. Allan, L. H. Baker, N. Bellouin, W. Collins, Z. Mousavi, and K. P. Shine (2016), Contrasting fast precipitation responses to tropospheric and stratospheric ozone forcing, *Geophys. Res. Lett.*, 43, 1263–1271, doi:10.1002/2015GL067231.

Received 3 DEC 2015

Accepted 7 JAN 2016

Accepted article online 9 JAN 2016

Published online 4 FEB 2016

©2016. The Authors.

This is an open access article under the terms of the Creative Commons Attribution License, which permits use, distribution and reproduction in any medium, provided the original work is properly cited.

# Contrasting fast precipitation responses to tropospheric and stratospheric ozone forcing

C. R. MacIntosh<sup>1</sup>, R. P. Allan<sup>1</sup>, L. H. Baker<sup>1</sup>, N. Bellouin<sup>1</sup>, W. Collins<sup>1</sup>, Z. Mousavi<sup>1</sup>, and K. P. Shine<sup>1</sup>
<sup>1</sup>Department of Meteorology, University of Reading, Reading, UK

**Abstract** The precipitation response to radiative forcing (RF) can be decomposed into a fast precipitation response (FPR), which depends on the atmospheric component of RF, and a slow response, which depends on surface temperature change. We present the first detailed climate model study of the FPR due to tropospheric and stratospheric ozone changes. The FPR depends strongly on the altitude of ozone change. Increases below about 3 km cause a positive FPR; increases above cause a negative FPR. The FPR due to stratospheric ozone change is, per unit RF, about 3 times larger than that due to tropospheric ozone. As historical ozone trends in the troposphere and stratosphere are opposite in sign, so too are the FPRs. Simple climate model calculations of the time-dependent total (fast and slow) precipitation change, indicate that ozone's contribution to precipitation change in 2011, compared to 1765, could exceed 50% of that due to CO<sub>2</sub> change.

## 1. Introduction

Recent research [e.g., *Allen and Ingram*, 2002; *Ming et al.*, 2010; *O'Gorman et al.*, 2012] has created a framework, based on energetic constraints, for understanding the global precipitation response to climate perturbations. A simple model has been developed [e.g., *Allan et al.*, 2014; *Ming et al.*, 2010; *Thorpe and Andrews*, 2014] that relates the component of top-of-atmosphere radiative forcing (RF) that directly affects the atmosphere (RF<sub>atm</sub>), surface temperature change ( $\Delta T$ ) and global-mean precipitation change ( $\Delta P$ ). This distinguishes between a *slow* precipitation response (SPR), related to  $\Delta T$  and a *fast* precipitation response (FPR), involving rapid atmospheric adjustments over a period of days and months, related to RF<sub>atm</sub> and the fast response of surface sensible heat (SH) fluxes ( $\Delta SH_{fast}$ ), so that

$$L\Delta P = SPR + FPR \approx k\Delta T - (RF_{atm} + \Delta SH_{fast}). \quad (1)$$

$L$  is the latent heat of vaporization and  $k$  is a model-dependent constant. This relationship arises because, to first order, net radiative cooling is balanced by latent heating due to condensation [e.g., *Mitchell et al.*, 1987]. In steady state, the net rate of condensation equals the global-mean precipitation. In response to a forcing, the net atmospheric radiative cooling (and hence the precipitation) responds to both RF<sub>atm</sub> and the subsequent climate response.

We consider RF<sub>atm</sub> in terms of RF using a parameter  $f$  (so that  $f = RF_{atm}/RF$ ) which is the fraction of RF felt directly by the atmosphere;  $k\Delta T$  represents the slow response arising from changes in atmospheric temperature, humidity, and cloudiness due to  $\Delta T$ .  $k$  can be derived from climate model simulations and may incorporate the slow SH response [Lambert and Webb, 2008; Andrews et al., 2010].  $\Delta SH_{fast}$  is normally smaller than  $L\Delta P$  and was not included in previous analyses [e.g., *Allan et al.*, 2014; *Thorpe and Andrews*, 2014] but will be computed here. We use two forms of RF [Myhre et al., 2013]. The more traditional RF (with stratospheric temperature adjustment) is used for illustrative calculations in section 2. Effective RF (ERF), which accounts for fast atmospheric adjustments to RF, is used in climate model simulations in section 3.

Climate model simulations [Andrews et al., 2010; Kvalevåg et al., 2013] show that  $f$  depends on the species under consideration. To our knowledge, Andrews et al. [2010] is the only study to quantify  $f$  for ozone. For total (preindustrial to present-day) ozone changes they found that  $f$  was negative (−0.3) and so FPR and SPR have the same sign (assuming  $\Delta SH_{fast}$  to be small); by contrast, they found  $f = 0.8$  for CO<sub>2</sub>, so that FPR opposes SPR. Ozone's potential importance can be illustrated by computing the equilibrium  $\Delta P$  to present-day RF; from equation (1) this is  $RF(k\lambda - f)$  (neglecting  $\Delta SH_{fast}$  for simplicity) [Shine et al., 2015], where  $\lambda$  is the climate sensitivity parameter. Using the Andrews et al. [2010]  $f$  factors, the 2011 RF values from Myhre et al. [2013] for total ozone and CO<sub>2</sub> (0.35 and 1.82 W m<sup>−2</sup>, respectively), a midrange  $\lambda$  of 0.8 K (W m<sup>−2</sup>)<sup>−1</sup> (assuming it is the same for

ozone and  $\text{CO}_2$ ) and  $k = 2.2 \text{ K (W m}^{-2})^{-1}$  (see section 4), ozone's equilibrium  $\Delta P$  is about 40% that of  $\text{CO}_2$ ; this is disproportionately strong compared to the RF (and equilibrium  $\Delta T$ ), where ozone's effect is 20% that of  $\text{CO}_2$ .

This letter distinguishes, for the first time, between the FPR for stratospheric and tropospheric ozone perturbations and explains their combined response. This is important as the time variation of stratospheric and tropospheric ozone, and their RF, is quite different [e.g., Myhre *et al.*, 2013] because they respond to different drivers; hence, a single value of  $f$  for ozone is unlikely to be applicable at all times. We first use radiation-only calculations to illustrate how  $\text{RF}_{\text{atm}}$  depends on the height of the ozone perturbation. These provide a platform for interpreting the response of an atmospheric general circulation model (GCM) which explicitly simulates the FPR. The first set of GCM calculations uses idealized ozone perturbations, particularly to explore the opposing FPR for lower and upper tropospheric ozone change and the amplified impact of stratospheric ozone changes, which are suggested by the radiation-only calculations. The second set uses more realistic ozone perturbations to quantify the FPR in response to historical ozone changes and to derive representative values for  $f$ . We then use these values in a simple global-mean model of historical precipitation change which includes both the FPR and SPR (equation (1)) to contrast the roles of tropospheric and stratospheric ozone change and compare them with  $\text{CO}_2$ .

This paper focuses largely on the relationship between global precipitation response and the global atmospheric energy balance. Ozone forcing can, via both the global response and changes in local circulation, induce changes in regional precipitation that are discussed elsewhere [e.g., Kang *et al.*, 2011; Shindell *et al.*, 2012; Marvel and Bonfils, 2013; Delworth and Zeng, 2014]. These papers stress that the precipitation response can be remote from the location of  $\text{RF}_{\text{atm}}$  and Muller and O'Gorman [2011] demonstrate how  $\text{RF}_{\text{atm}}$  and precipitation changes can be locally uncorrelated due to changes in horizontal transport of moisture and energy; in the present context, Kang *et al.* [2011] and Delworth and Zeng [2014] show how Antarctic ozone depletion can influence tropical and subtropical precipitation patterns, by causing a poleward shift in the midlatitude jet and an associated shift in the Hadley cell. Thus, an understanding of the local precipitation response requires an understanding of the impact of changes in the convergence and divergence of atmospheric moisture and energy.

## 2. Atmospheric Radiative Forcing as a Function of the Altitude of Ozone Perturbation

Assuming that the thermal infrared is the most height-dependent component of RF (as will be shown below), a simple conceptual model can be used to anticipate the response. The net effect of an increase in ozone depends on competition between increased atmospheric absorption of surface-emitted radiation (causing a positive  $\text{RF}_{\text{atm}}$ ) and increased atmospheric emission (causing a negative  $\text{RF}_{\text{atm}}$ ). In the warm lower troposphere, the emission term is likely the largest; in the colder upper troposphere, the absorption term is likely more important. Simple grey body considerations (see supporting information) indicate that the  $\text{RF}_{\text{atm}}$  is likely to change sign in the midtroposphere. Such a sign change (at around 700 hPa) has previously been shown, using detailed calculations, in response to increased water vapor amounts [Previdi, 2010].

A set of idealized radiation-only perturbation experiments are performed in which ozone is increased by 20% in each atmospheric layer in turn. RF,  $\text{RF}_{\text{atm}}$ , and  $f$  are calculated for both cloud-free and all-sky cases using the Edwards and Slingo [1996] radiation code with nine longwave and six shortwave spectral bands. The day-averaged shortwave calculations use midmonth conditions and a six-point Gaussian integration over daylight hours. Calculations are performed on a  $2.5^\circ \times 3.75^\circ$  horizontal grid at 22 levels, using temperatures and humidity climatologies described in MacIntosh *et al.* [2015]. The zonal-mean ozone distribution is taken from the Atmospheric Chemistry and Climate Model Intercomparison Project (ACCMIP) multimodel mean (not including the MOCAGE model in the stratosphere, where it is an outlier) [Young *et al.*, 2013] and is based on year 2000 ozone precursor emissions and concentrations of ozone-depleting substances. Stratospheric temperature adjustment is applied using fixed dynamical heating with a  $2 \text{ K km}^{-1}$  tropopause definition. Annual means are derived from averaging monthly mean calculations for January, April, July, and October. Some sensitivity to these specifications can be anticipated, but the prime purpose is to illustrate the driving physics, to help anticipate and interpret the GCM calculations in section 3.

Figure 1a shows the strong dependence of  $\text{RF}_{\text{atm}}$  on the height of ozone perturbation, with only a small dependence on whether clouds are present. The variation with height in the troposphere is largely driven

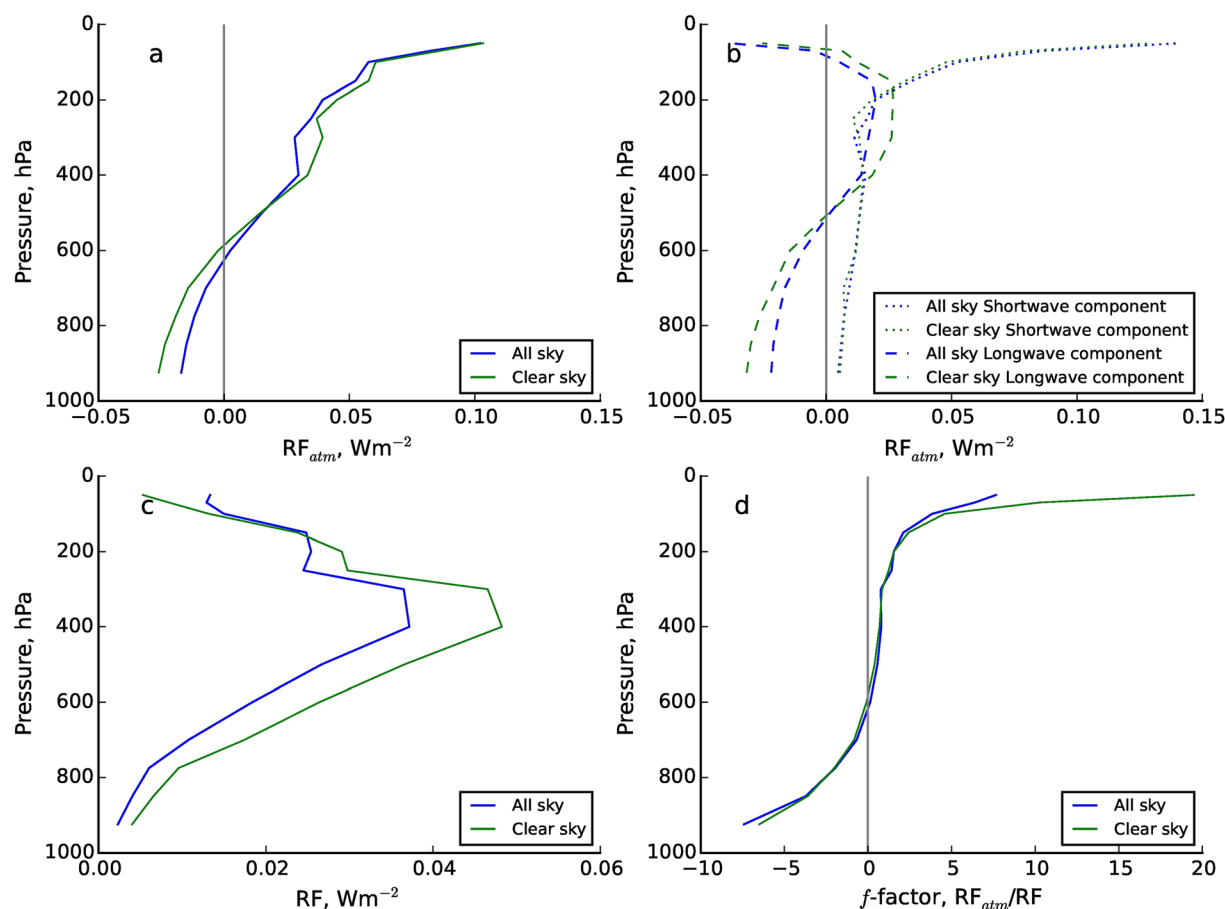


**Figure 1.** Impact of 20% global increases in ozone applied in each atmospheric layer in turn on  $RF_{atm}$ ,  $RF$ , and  $f$ . The vertical coordinate is the pressure at which the perturbation is applied. (a)  $RF_{atm}$ ; (b) longwave (including stratospheric adjustment) and shortwave components of Figure 1a; (c)  $RF$ ; (d)  $f = RF_{atm}/RF$ . Results are shown for clear sky and all-sky cases.

by the longwave (Figure 1b). However, the shortwave perturbation strongly modifies where  $RF_{atm}$  changes sign and its magnitude, particularly in the upper troposphere and lower stratosphere.  $RF$  itself (Figure 1c) also depends on the height of the ozone perturbation, but it remains positive throughout the troposphere and lower stratosphere; it only becomes negative in the upper stratosphere [e.g., *Lacis et al.*, 1990] above the region of interest here. Hence,  $f$  depends strongly on the vertical distribution of ozone change (Figure 1d) and changes sign at about 650 hPa. Because  $\Delta T$ , driven by  $RF$ , is positive for an ozone increase, the associated FPR will enhance the SPR for lower tropospheric ozone increases but oppose it for increases at higher altitudes.

For stratospheric ozone increases, the atmosphere as a whole gains energy due to increased shortwave (SW) absorption; this is opposed by increased longwave (LW) emission, mostly as a result of the increase in stratospheric temperature in response to the SW absorption. Further analysis shows that the tropospheric energy gain, in this case, is primarily due to increased LW emission from the warmed stratosphere, as the SW absorbed by the troposphere decreases for this case. For tropospheric ozone increases, the increased SW absorption results in a tropospheric energy gain; whether the atmosphere as a whole gains or loses LW energy depends on the altitude of the ozone change.

### 3. Climate Model Simulations of the Fast Precipitation Response to Ozone Change

We test the link between ERF and FPR using the atmosphere-only version of the HadGEM3 climate model, with a resolution of  $1.875^\circ \times 1.25^\circ$  and 63 vertical levels between the surface and 40 km [Hewitt et al., 2011]. It also uses the *Edwards and Slingo* [1996] radiation scheme. Model winds above the boundary layer are relaxed toward ERA-Interim analyses following the method of *Telford et al.* [2008]. This experimental setup allows relatively short model integrations which produce ERFs very similar to those from longer (20 year)

**Table 1.** Top-Of-Atmosphere and Atmospheric Effective Radiative Forcing, the Fast Sensible Heat Flux Change, Fast Precipitation Response (Multiplied by the Latent Heat of Vaporization) (All in  $\text{W m}^{-2}$ ), and  $f$  (i.e.,  $\text{ERF}_{\text{atm}}/\text{ERF}$ ) for Climate Model Simulations for Four Idealized and Three More Realistic Ozone Perturbations<sup>a</sup>

Experiment	$\text{ERF}(\text{W m}^{-2})$	$\text{ERF}_{\text{atm}}(\text{W m}^{-2})$	$\Delta\text{SH}_{\text{fast}}(\text{W m}^{-2})$	$\text{ERF}_{\text{atm}} + \Delta\text{SH}_{\text{fast}}(\text{W m}^{-2})$	$\text{FPR}(\text{W m}^{-2} \text{ and } \text{mm day}^{-1})$	$f$
<i>Idealized</i>						
UT + LT	$1.11 \pm 0.01$	$0.48 \pm 0.01$	$-0.11 \pm 0.01$	$0.37 \pm 0.01$	$-0.37 \pm 0.01$ (−0.013)	$0.43 \pm 0.01$
LT	$0.28 \pm 0.01$	$-0.12 \pm 0.01$	$0.02 \pm 0.01$	$-0.10 \pm 0.00$	$0.10 \pm 0.00$ (0.0034)	$-0.42 \pm 0.03$
UT	$0.83 \pm 0.01$	$0.58 \pm 0.01$	$-0.13 \pm 0.01$	$0.46 \pm 0.01$	$-0.45 \pm 0.00$ (−0.015)	$0.70 \pm 0.01$
ST	$-0.27 \pm 0.02$	$-0.46 \pm 0.02$	$0.10 \pm 0.00$	$-0.36 \pm 0.01$	$0.36 \pm 0.02$ (0.012)	$1.70 \pm 0.10$
<i>More Realistic</i>						
FULL	$0.26 \pm 0.02$	$0.006 \pm 0.002$	$-0.009 \pm 0.005$	$-0.003 \pm 0.007$	$0.005 \pm 0.011$ (0.0017)	$0.02 \pm 0.01$
TROP	$0.36 \pm 0.00$	$0.13 \pm 0.01$	$-0.03 \pm 0.00$	$0.10 \pm 0.00$	$-0.10 \pm 0.01$ (−0.0034)	$0.36 \pm 0.01$
STRAT	$-0.096 \pm 0.026$	$-0.12 \pm 0.01$	$0.02 \pm 0.01$	$-0.10 \pm 0.01$	$0.10 \pm 0.01$ (0.0034)	$1.27 \pm 0.36$

<sup>a</sup>The fast precipitation response in  $\text{mm day}^{-1}$  is shown in parentheses. The results are the average of 3 years; the  $\pm$  range encompasses the values for each individual year.

integrations using an unconstrained model (Bellouin et al., manuscript in preparation, 2016). By not relaxing temperatures, the fast adjustments are less constrained, but there will be some suppression of the dynamical response. Simulations are run for 3 years (2008–2010) with sea surface temperatures (SSTs) and sea ice from the Atmospheric Model Intercomparison Project climatology [Reynolds et al., 2007]. Fixing SSTs inhibits the SPR, although land temperatures remain free to adjust. ACCMIP ozone fields (section 2) were imposed as monthly varying zonal-mean climatologies. Forcings are presented as 3 year averages; the range that encompasses the forcings for individual years is shown to indicate the robustness of the 3 year mean.

### 3.1. Idealized Ozone Perturbations

A control simulation was conducted with the year 2000 ACCMIP ozone climatology (section 2). Idealized simulations were then run by doubling ozone mixing ratios between the surface and 700 hPa (labeled Lower Troposphere, LT), between 700 hPa and the tropopause (Upper Troposphere, UT), and between the surface and the tropopause (LT + UT) to test the additivity of the UT and LT responses. For the stratosphere perturbation (ST) ozone mixing ratios were decreased by 20% between the tropopause and the model top. The  $150 \text{ nmol mol}^{-1}$  ozone contour was used to identify the tropopause in the simulations.

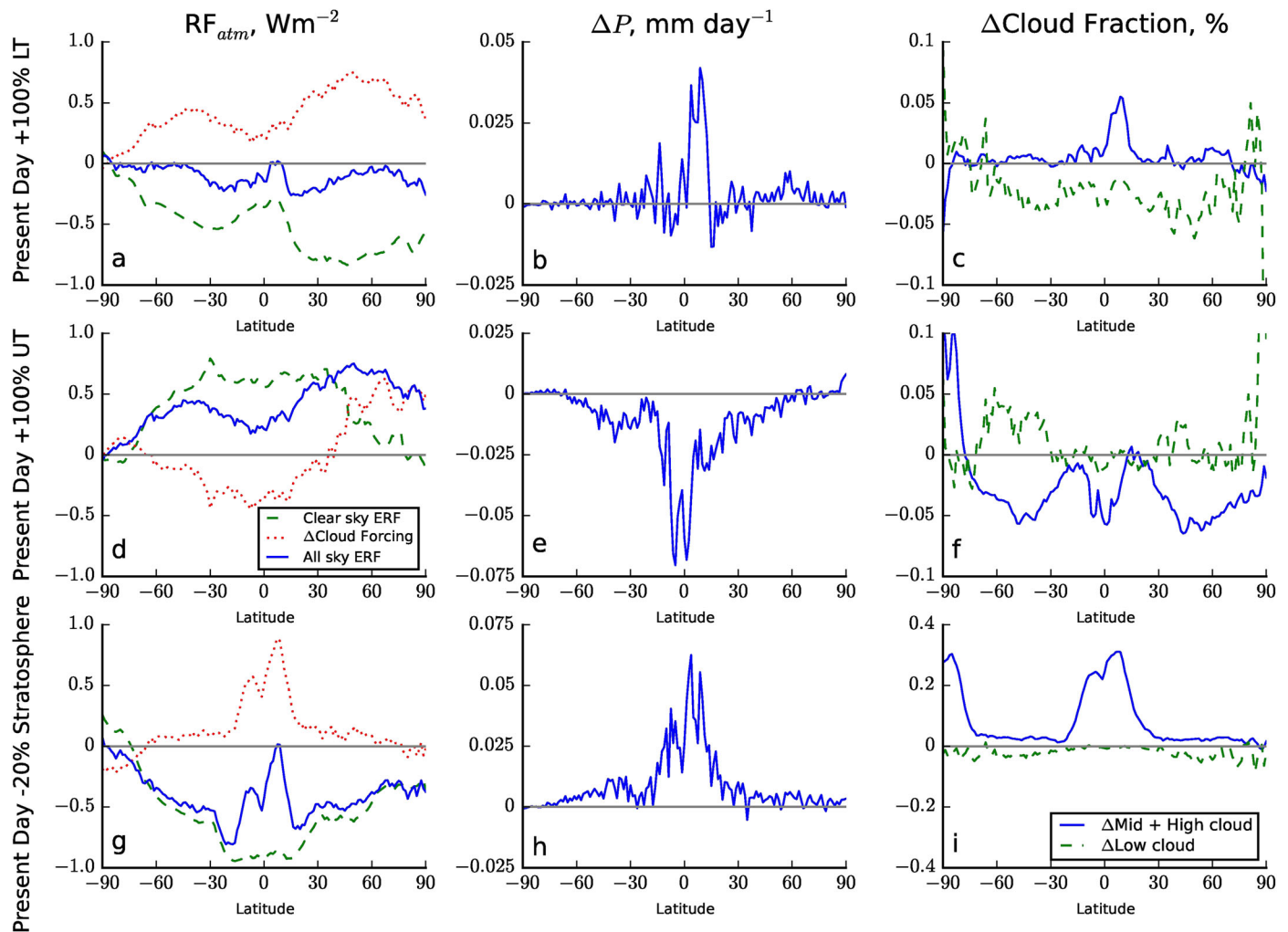
Table 1 shows the global-mean results for these experiments for ERF,  $\text{ERF}_{\text{atm}}$ ,  $\Delta\text{SH}_{\text{fast}}$  and  $f$  (from  $\text{ERF}_{\text{atm}}/\text{ERF}$ ). The validity of the simple FPR model (equation (1)) is assessed by comparing the predicted FPR due to  $\text{ERF}_{\text{atm}} + \Delta\text{SH}_{\text{fast}}$  with the GCM-simulated change in precipitation (converted to units of  $\text{W m}^{-2}$ ).

Table 1 shows that LT causes a positive FPR whereas UT causes a negative FPR despite ERF being positive for both cases. The ST experiment causes a positive FPR; because this is for an ozone decrease, the sense of the response (ozone increase leads to negative FPR) is the same as for UT.  $\text{ERF}_{\text{atm}} + \Delta\text{SH}_{\text{fast}}$  predict this behavior well, supporting the utility of equation (1);  $\Delta\text{SH}_{\text{fast}}$  is quite significant in size, typically 20–30% of  $\Delta\text{LP}$ . The sign difference between the LT and UT FPR is as anticipated from Figure 1, showing that the behavior is understood. LT + UT is within 5% of the sum of LT and UT and shows that UT dominates.  $f$  varies strongly with height; it is largest for ST and positive in all cases except LT. The FPR for ST is, per unit ERF, roughly 4 times larger than the FPR for LT + UT.

We briefly discuss the annual- and zonal-mean latitudinal distribution of FPR and the role of cloud changes in influencing ERF. Figures 2a, 2d, and 2g show the structure of  $\text{ERF}_{\text{atm}}$  (for clear-sky and all-sky cases) and the change in cloud radiative forcing between the control and perturbed cases. Clear- and all-sky ozone forcings differ, because clouds strongly modulate the shortwave and longwave RF [e.g., Bernsten et al., 1997]. Here the GCM results illustrate a marked difference between clear- and all-sky ERFs (shown by the change in cloud forcing), particularly for LT (Figure 2a), which is larger than anticipated from the RF calculations (Figure 1). This indicates a significant fast cloud adjustment to the ozone perturbation, which modifies the  $\text{ERF}_{\text{atm}}$  and acts in addition to  $\text{RF}_{\text{atm}}$ .

Figures 2b, 2e, and 2h show that precipitation changes occur largely in the tropics in all cases and illustrate further the contrasting response of precipitation to LT and UT/ST ozone changes. Figures 2c, 2f, and 2i show indicators of cloud response in the model, the change in middle plus high and low cloud fraction (to distinguish between cloud within and above the boundary layer). The response is complex and merits detailed study, but for all three simulations, a similar signature to the tropical precipitation change can clearly be seen in the middle plus high cloud fraction.





**Figure 2.** (a, d, and g) Zonal and annual-mean ERFs, (b, e, and h) precipitation changes, and (c, f, and i) cloud changes for the idealized ozone perturbation GCM simulations. Cloud responses are separated between below 2 km (“low”) and above 2 km (“Mid + High”). The LT, UT, and ST simulations are in the top, middle, and bottom rows, respectively.

### 3.2. More Realistic Ozone Perturbations

We now consider more realistic ozone changes between the preindustrial (1850) and the present-day (2000) atmosphere, derived from ACCMIP multimodel means (see section 2). The control simulation uses 1850 ozone. Three perturbations are performed. “TROP” uses year 2000 tropospheric ozone; “STRAT” uses year 2000 ozone above the tropopause; “FULL” uses year 2000 ozone throughout the atmosphere. Since GCM runs are inherently noisy, we increased the TROP forcing to amplify the signal, by perturbing ozone by twice its historical change. The results presented here are divided by two; we tested the linearity via off-line radiation calculations; for ozone perturbations of this size,  $RF_{atm}$  is linear to better than 1%.

Table 1 shows that TROP causes a negative FPR. Hence, for more realistic ozone changes, as well as the idealized ones (section 3.1), upper tropospheric changes are more influential than lower troposphere changes. STRAT causes a positive FPR and, as in the idealized experiments,  $f$  is much larger (by about a factor of 3 here) than for tropospheric ozone changes. The FULL FPR is approximately the sum of the individual STRAT plus TROP experiments.  $ERF_{atm} + \Delta SH_{fast}$  is again a good indicator of FPR, with  $\Delta SH_{fast}$  accounting for 20–30% of  $\Delta P$ . Figure S2 shows the equivalent plot to Figure 2 for these simulations and has broadly the same patterns; the signal is noisier because ozone and ERF changes are smaller (see Table 1). In the STRAT case while  $ERF_{atm}$  is predominantly at high southern latitudes, the response is largely in the tropics; this emphasizes that while the global energetic constraint explains global-mean precipitation response (Table 1), the relationship does

not hold locally, even to the extent that the sign of the local  $\text{ERF}_{\text{atm}}$  does not predict the sign of the local precipitation response (see also *Muller and O'Gorman* [2011]).

The resulting FULL  $\text{ERF}_{\text{atm}}$  is positive but small, and  $f$  is close to zero. The FPR due to stratospheric and tropospheric ozone changes strongly oppose each other in present-day conditions, despite the tropospheric ozone ERF being about 3.5 times the stratospheric ozone ERF.

These results contrast with *Andrews et al.* [2010] who find a net ozone RF of  $0.16 \text{ W m}^{-2}$  for the preindustrial to 1990 period (compared to  $0.26 \text{ W m}^{-2}$  found here for FULL), and  $f$  of  $-0.3$ ; this suggests that, in their calculation, stratospheric ozone depletion is a larger component of RF. The sign of  $f$  for combined stratosphere and troposphere ozone forcings does not have to be positive, even though the individual  $f$  factors (Table 1) are. This is because although the tropospheric ozone ERF dominates over the stratospheric ozone ERF (making the net ERF positive) this is not the case for  $\text{ERF}_{\text{atm}}$ ; these are of comparable size but opposite signs, making the sign of  $\text{ERF}_{\text{atm}}$  uncertain. Hence, if the stratospheric component were larger than calculated here,  $f$  could be negative, as found by *Andrews et al.* [2010].

We are unaware of any other ERF calculations for ozone, but our ERFs are broadly consistent with the RFs in *Stevenson et al.* [2013] and *Conley et al.* [2013] as used in *Myhre et al.* [2013]. For tropospheric ozone *Stevenson et al.* [2013] give an RF of  $0.34 \text{ W m}^{-2}$  for the same 1850–2000 data set compared with our ERF of  $0.36 \text{ W m}^{-2}$ . For stratospheric ozone *Conley et al.* [2013] calculate an RF of  $-0.02 \text{ W m}^{-2}$  using a single radiation code applied to ozone changes from several ACCMIP models; *Myhre et al.* [2013] assess the 1750–2011 RF to be  $-0.05$  (range  $-0.15$  to  $+0.05 \text{ W m}^{-2}$ ) compared with the ERF of  $-0.1 \text{ W m}^{-2}$  derived here.

Repeating the equilibrium  $\Delta P$  calculation in section 1, but using the  $f$  values derived here for stratospheric and tropospheric ozone (and the separate 2011 RFs of  $0.05$  and  $0.40 \text{ W m}^{-2}$ , respectively [*Myhre et al.*, 2013]) yields a reduced proportion to the  $\text{CO}_2$  change of 33% compared to 40% in section 1, because the FPR no longer enhances the SPR. Nevertheless, this remains disproportionately strong compared to the RFs.

#### 4. Simple Model Calculations of Total Precipitation Response

To investigate the impact of these  $f$  values on the time-varying total precipitation response, we use the simple model approach of *Allan et al.* [2014] which incorporates the SPR and FPR. As in *Thorpe and Andrews* [2014] and *Allan et al.* [2014],  $\Delta\text{SH}_{\text{fast}}$  is not included, given the illustrative nature of the calculations, but could reduce the ozone FPR by about 20%.

To compute the time-varying SPR, temperature is calculated with a simple global-mean model, with a mixed layer ocean connected to a deep ocean via diffusion. These temperatures, and the  $f$  values from section 3.2, are used to calculate the precipitation response using equation (1). A midrange climate sensitivity of  $0.8 \text{ K (W m}^{-2})^{-1}$  [*Intergovernmental Panel on Climate Change (IPCC)*, 2013] is used (and assumed to be the same for all forcing components).  $k$  is taken to be  $2.2 \text{ W m}^{-2} \text{ K}^{-1}$ , consistent with the multimodel mean value in *Previdi* [2010] and *Thorpe and Andrews* [2014] and includes the slow component of  $\Delta\text{SH}$ . The SPR, and hence the relative importance of the FPR, depends strongly on the choice of  $\lambda$  [e.g., *Shine et al.*, 2015] and  $k$ .

The 1765–2011 tropospheric and stratospheric ozone RFs are taken from *IPCC* [2013 Appendix AII.1.2]. These are used to directly calculate the time-varying FPR; as explained in section 3.2, these do not exactly correspond to the forcings derived from the more-realistic ozone GCMs perturbations, so the present-day FPRs differ slightly from Table 1 (and differ because  $\Delta\text{SH}_{\text{fast}}$  is neglected in the simple model). The precipitation response is compared with that for  $\text{CO}_2$  (assuming  $f = 0.8$  [*Andrews et al.*, 2010] and the *IPCC* [2013]  $\text{CO}_2$  RFs) and for ozone but assuming the *Andrews et al.* [2010]  $f = -0.3$  for both tropospheric and stratospheric ozone.

Figure 3a shows the total ozone-related precipitation response and the FPR using  $f = -0.3$ . In this case, the tropospheric ozone FPR is positive, enhancing the SPR, while the stratospheric ozone FPR and total response is negative. Figure 3b is the same as Figure 3a but uses the new  $f$  values for tropospheric and stratospheric ozone. In contrast to Figure 3a, since the tropospheric ozone FPR now opposes the SPR, the total response is reduced, by a quarter in 2011. By contrast, the FPR is so strong for stratospheric ozone that it overwhelms the SPR, causing a small precipitation increase. Figure 3c shows the SPR and FPR for  $\text{CO}_2$  and tropospheric ozone using the  $f$  value derived here, to emphasize the strong compensation between the SPR and FPR components for  $\text{CO}_2$ .



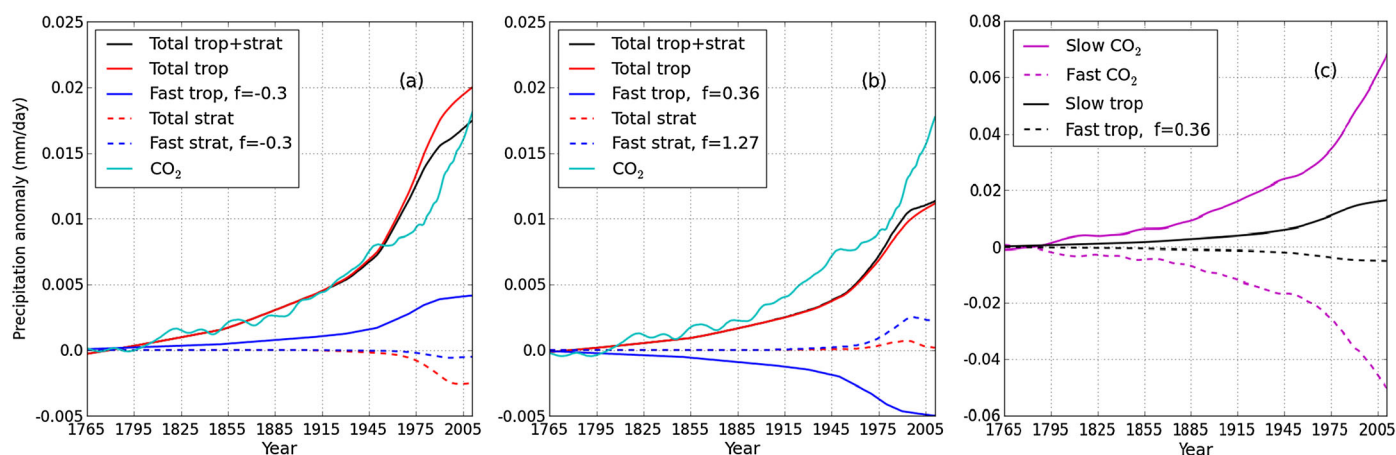


**Figure 3.** Simple model estimates of the global-mean precipitation response to ozone forcing using the IPCC AR5 radiative forcings from 1765 to 2010. (a) Total and fast precipitation response to tropospheric, stratospheric ozone and both using  $f = -0.3$ . The total response to  $\text{CO}_2$  is also shown. (b) As in Figure 3a but using  $f = 0.36$  for tropospheric and  $f = 1.27$  for stratospheric ozone. (c) The fast and slow components of the response for  $\text{CO}_2$  and tropospheric ozone.

Although the total ozone  $\Delta P$  is now smaller than when using  $f = -0.3$ , Figure 3b shows that it remains a large fraction of the  $\text{CO}_2$   $\Delta P$  (about 70% in 2011) despite the RF being only about 20% that of  $\text{CO}_2$ . It is also significantly stronger than the value of 33% of equilibrium  $\Delta P$  derived in section 3.2. This is because, in a transient calculation, the SPR, which drives the positive  $\Delta P$  for  $\text{CO}_2$  and tropospheric ozone, is not fully expressed (unlike the FPR), as the temperature change is not in equilibrium with the RF. Since the FPR is proportionately more important in suppressing precipitation for  $\text{CO}_2$  than tropospheric ozone, (Figure 3c), the ozone total  $\Delta P$  is a larger fraction of that for  $\text{CO}_2$  in the transient case. The relative importance of tropospheric ozone is also slightly larger, because in 2011, its  $\Delta T$  (and hence its SPR) is closer to equilibrium (about 67%) than  $\text{CO}_2$  (about 60%) because the ozone forcing is, in relative terms, increasing less rapidly than the  $\text{CO}_2$  forcing.

The results emphasize the need to treat tropospheric and stratospheric ozone separately in simple models. The time variation of stratospheric ozone can be seen to have some influence on recent precipitation changes, accelerating it (relative to the troposphere-only case) during the 1980s, and opposing it after 2000. Using the “compound” value of  $f$  for present-day ozone forcing (about 0.02 from Table 1) would misrepresent the time evolution of the FPR, as it would be close to zero throughout the time period in Figure 3.

## 5. Discussion

This work has presented the first detailed climate model calculations of the FPR for tropospheric and stratospheric ozone changes and further demonstrates the primary role of the atmospheric energy constraint in driving the FPR. As is clear from Table 1, across all the GCM experiments discussed here,  $\Delta \text{SH}_{\text{fast}}$  offsets about 20% of the FPR that would result directly from  $\text{RF}_{\text{atm}}$ . This almost constant proportion contrasts with the absorbing aerosol case of Ming *et al.* [2010] where  $\Delta \text{SH}$  (and, they argue,  $\Delta \text{SH}_{\text{fast}}$ ) became the dominant term in balancing  $\text{RF}_{\text{atm}}$  when aerosol was located in the boundary layer. The contrasting behavior may be because our ozone perturbations are rather deep (extending to 700 hPa in the LT case) or it may be related to the differences in the impact of ozone and aerosol on  $\text{RF}_{\text{atm}}$ .

This study demonstrates that the FPR for changes in lower tropospheric ozone has the same sign as the SPR, while for upper tropospheric and stratospheric ozone changes, it is of opposite sign. Radiation-only calculations demonstrate the reasons that originate in the balance between the change in absorption and emission of infrared radiation modified by the change in absorption of solar radiation. For more realistic ozone changes, the FPR for tropospheric ozone overall acts to oppose the SPR, as it does for stratospheric ozone; however, since the historical changes in tropospheric and stratospheric ozone (and their RFs) are of opposite signs, so too are their FPRs. Per unit radiative forcing, the FPR for stratospheric ozone changes are found to be 3 to 4 times larger than the tropospheric ozone FPR.

A simple model of the time-varying global-mean precipitation change, including the FPR and SPR, indicates that, for the model parameters chosen here, the present-day precipitation response to ozone change may

exceed 50% of that due to CO<sub>2</sub>, even though the RF is only about 20%. This is mostly because the compensation between the FPR and SPR is much stronger for CO<sub>2</sub> than tropospheric ozone and partly because stratospheric ozone depletion, despite its negative RF, causes precipitation increases. The results also indicate that, in simple model approaches, it is important to treat tropospheric and stratospheric ozone separately; the total ozone FPR depends on the balance of the strength of the individual tropospheric and stratospheric RFs which is very time dependent.

Clearly, the analysis presented here is for a single GCM and for particular ozone perturbations; the response of other climate models would be of great interest. It also focuses on the global, rather than regional, responses. Nevertheless, the results highlight the opposing roles of stratospheric and tropospheric ozone in the FPR, the efficacy of stratospheric ozone in causing an FPR, and show that the overall impact of ozone change on global precipitation response may be substantial.

# Acknowledgments

C.M., L.B., N.B., W.C., and K.S. were supported by the European Commission's ECLIPSE (Evaluating the Climate and Air Quality Impacts of Short-Lived Pollutants) Project (grant agreement 282688). R.A. was supported by the UK Natural Environment Research Council DEEP-C project (NE/K005480/1) and the National Centre for Atmospheric Sciences. Tim Andrews and an anonymous reviewer are thanked for many helpful comments. Data used as input to the model calculations in this study are properly cited and referred to in the reference list. The model output data presented here are available from the corresponding author upon request.

# References

- Allan, R. P., C. L. Liu, M. Zahn, D. A. Lavers, E. Koukouvasias, and A. Bodas-Salcedo (2014), Physically consistent responses of the global atmospheric hydrological cycle in models and observations, *Surv. Geophys.*, *35*, 533–552, doi:10.1007/s10712-012-9213-z.
- Allen, M. R., and W. J. Ingram (2002), Constraints on future changes in climate and the hydrologic cycle, *Nature*, *419*, 224–232, doi:10.1038/nature01092.
- Andrews, T., P. M. Forster, O. Boucher, N. Bellouin, and A. Jones (2010), Precipitation, radiative forcing and global temperature change, *Geophys. Res. Lett.*, *37*, L14701, doi:10.1029/2010GL043991.
- Berntsen, T., I. Isaksen, G. Myhre, J. Fuglestad, F. Stordal, T. Larsen, R. Freckleton, and K. Shine (1997), Effects of anthropogenic emissions on tropospheric ozone and its radiative forcing, *J. Geophys. Res.*, *102*, 28,101–28,126, doi:10.1029/97JD02226.
- Conley, A. J., J. F. Lamarque, F. Vitt, W. D. Collins, and J. Kiehl (2013), PORT, a CESM tool for the diagnosis of radiative forcing, *Geosci. Model Dev.*, *6*, 469–476, doi:10.5194/gmd-6-469-2013.
- Delworth, T. L., and F. R. Zeng (2014), Regional rainfall decline in Australia attributed to anthropogenic greenhouse gases and ozone levels, *Nat. Geosci.*, *7*, 583–587, doi:10.1038/ngeo2201.
- Edwards, J. M., and A. Slingo (1996), Studies with a flexible new radiation code. 1: Choosing a configuration for a large-scale model, *Q. J. R. Meteorol. Soc.*, *122*, 689–719, doi:10.1002/qj.49712253107.
- Hewitt, H. T., D. Copsey, I. D. Culverwell, C. M. Harris, R. S. R. Hill, A. B. Keen, A. J. McLaren, and E. C. Hunke (2011), Design and implementation of the infrastructure of HadGEM3: The next-generation Met Office climate modelling system, *Geosci. Model Dev.*, *4*, 223–253, doi:10.5194/gmd-4-223-2011.
- Intergovernmental Panel on Climate Change (IPCC) (2013), *Climate Change 2013: The Physical Science Basis. Contribution of Working Group I to the Fifth Assessment Report of the Intergovernmental Panel on Climate Change*, 1535 pp., Cambridge Univ. Press, Cambridge, U. K., and New York.
- Kang, S. M., L. M. Polvani, J. C. Fyfe, and M. Sigmond (2011), Impact of polar ozone depletion on subtropical precipitation, *Science*, *332*, 951–954, doi:10.1126/science.1202131.
- Kvalevåg, M. M., B. H. Samset, and G. Myhre (2013), Hydrological sensitivity to greenhouse gases and aerosols in a global climate model, *Geophys. Res. Lett.*, *40*, 1432–1438, doi:10.1002/grl.50318.
- Lacis, A. A., D. J. Wuebbles, and J. A. Logan (1990), Radiative forcing of climate by changes in the vertical-distribution of ozone, *J. Geophys. Res.*, *95*, 9971–9981, doi:10.1029/JD095iD07p09971.
- Lambert, F. H., and M. J. Webb (2008), Dependency of global mean precipitation on surface temperature, *Geophys. Res. Lett.*, *35*, L16706, doi:10.1029/2008GL034838.
- MacIntosh, C. R., K. P. Shine, and W. J. Collins (2015), Radiative forcing and climate metrics for ozone precursor emissions: The impact of multi-model averaging, *Atmos. Chem. Phys.*, *15*, 3957–3969, doi:10.5194/acp-15-3957-2015.
- Marvel, K., and C. Bonfils (2013), Identifying external influences on global precipitation, *Proc. Natl. Acad. Sci. U.S.A.*, *110*, 19,301–19,306, doi:10.1073/pnas.1314382110.
- Ming, Y., V. Ramaswamy, and G. Persad (2010), Two opposing effects of absorbing aerosols on global-mean precipitation, *Geophys. Res. Lett.*, *37*, L13701, doi:10.1029/2010GL042895.
- Mitchell, J. F. B., C. A. Wilson, and W. M. Cunningham (1987), On CO<sub>2</sub> climate sensitivity and model dependence of results, *Q. J. R. Meteorol. Soc.*, *113*, 293–322, doi:10.1256/smsqj.47516.
- Muller, C. J., and P. A. O'Gorman (2011), An energetic perspective on the regional response of precipitation to climate change, *Nat. Clim. Change*, *1*, 266–271, doi:10.1038/nclimate1169.
- Myhre, G., et al. (2013), Anthropogenic and Natural Radiative Forcing, in *Climate Change 2013: The Physical Science Basis. Contribution of Working Group I to the Fifth Assessment Report of the Intergovernmental Panel on Climate Change*, edited by T. F. Stocker et al., pp. 659–740, Cambridge Univ. Press, Cambridge, U. K., and New York.
- O'Gorman, P. A., R. P. Allan, M. P. Byrne, and M. Previdi (2012), Energetic constraints on precipitation under climate change, *Surv. Geophys.*, *33*, 585–608, doi:10.1007/s10712-011-9159-6.
- Previdi, M. (2010), Radiative feedbacks on global precipitation, *Environ. Res. Lett.*, *5*, doi:10.1088/1748-9326/5/2/025211.
- Reynolds, R. W., T. M. Smith, C. Liu, D. B. Chelton, K. S. Casey, and M. G. Schlax (2007), Daily high-resolution-blended analyses for sea surface temperature, *J. Clim.*, *20*, 5473–5496, doi:10.1175/2007jcli1824.1.
- Shindell, D. T., A. Voulgarakis, G. Faluvegi, and G. Milly (2012), Precipitation response to regional radiative forcing, *Atmos. Chem. Phys.*, *12*, 6969–6982, doi:10.5194/acp-12-6969-2012.
- Shine, K. P., R. P. Allan, W. J. Collins, and J. S. Fuglestad (2015), Metrics for linking emissions of gases and aerosols to global precipitation changes, *Earth Syst. Dyn.*, *6*, 525–540, doi:10.5194/esd-6-525-2015.
- Stevenson, D. S., et al. (2013), Tropospheric ozone changes, radiative forcing and attribution to emissions in the Atmospheric Chemistry and Climate Model Intercomparison Project (ACCMIP), *Atmos. Chem. Phys.*, *13*, 3063–3085, doi:10.5194/acp-13-3063-2013.

- Telford, P. J., P. Braesicke, O. Morgenstern, and J. A. Pyle (2008), Technical note: Description and assessment of a nudged version of the new dynamics Unified Model, *Atmos. Chem. Phys.*, *8*, 1701–1712, doi:10.5194/acp-8-1701-2008.
- Thorpe, L., and T. Andrews (2014), The physical drivers of historical and 21st century global precipitation changes, *Environ. Res. Lett.*, *9*, doi:10.1088/1748-9326/9/6/064024.
- Young, P. J., et al. (2013), Pre-industrial to end 21st century projections of tropospheric ozone from the Atmospheric Chemistry and Climate Model Intercomparison Project (ACCMIP), *Atmos. Chem. Phys.*, *13*, 2063–2090, doi:10.5194/acp-13-2063-2013.